Appl Phys A (2014) 114:1309–1319
DOI 10.1007/s00339-013-7953-3

**Applied Physics A**
**Materials Science & Processing**

# Effect of crystal orientation on picosecond-laser bulk microstructuring and Raman lasing in diamond

**Sergei M. Pimenov · Beat Neuenschwander · Beat Jäggi · Valerio Romano**

Received: 19 July 2013 / Accepted: 26 August 2013 / Published online: 10 September 2013


**Abstract** In the paper we report on picosecond-laser bulk microstructuring and stimulated Raman scattering (SRS) in type IIa single-crystal diamond in the course of multipulse irradiation at $\lambda = 532$ nm wavelength using an advanced ps-laser system equipped with additional setups for on-line video imaging and photoluminescence spectra measurements. The effect of crystal orientation (relative to the incident laser beam) on (i) optical breakdown thresholds, (ii) character of bulk modifications, and (iii) generation of stimulated Raman scattering in diamond during irradiation with picosecond pulses of different durations ($\tau_1 = 10$ ps and $\tau_2 = 44$ ps) is studied. It is shown that the processes of laser-induced breakdown in the bulk of diamond (at the backside of the crystals) and bulk microstructure growth are governed by the dielectric breakdown mechanism. It is found that generation of high-order stimulated Raman scattering in diamond crystals has a considerable effect on the threshold of laser-induced breakdown and bulk microstructuring. Conditions of the efficient SRS lasing are determined, depending on the pulse duration and the direction ([100] and [110]) of the laser beam incidence. A method of local temperature measurements in the bulk of diamond based on the Stokes-to-anti-Stokes intensity ratio in the recorded SRS spectra is proposed, its applicability to determine a "pre-breakdown" temperature of diamond during multipulse ps-laser irradiation is discussed.

S.M. Pimenov (✉)
Natural Sciences Center, General Physics Institute, Moscow 119991, Russia
e-mail: pimenov@nsc.gpi.ru

B. Neuenschwander · B. Jäggi · V. Romano
Bern University of Applied Sciences, Engineering & Information Technology, Burgdorf 3400, Switzerland

B. Neuenschwander
e-mail: beat.neuenschwander@bfh.ch

V. Romano
e-mail: valerio.romano@bfh.ch

## 1 Introduction

Bulk microstructuring of diamond crystals using ultrashort pulse lasers is based on local structural modifications resulting from laser-induced optical breakdown in the material. In laser-induced breakdown of diamond, the process of avalanche ionization was reported to dominate in producing most of free electrons during irradiation with visible and near-infrared ultrashort pulses over the range from a few tens of picoseconds to 120 fs [1, 2], similarly to the laser-induced breakdown in other optically transparent materials [3, 4], while for UV ultrashort pulses the multiphoton absorption is the dominant process in generation of free carriers [5]. It is the ultrafast free electron generation (by avalanche or multiphoton ionization) and interaction of the excited electron system with the lattice that result in structural changes and ultrafast phase transitions (graphitization) in the bulk of diamond [6, 7]. There have been several experimental studies reported on the bulk microstructuring of single-crystal diamond [8–16] which were mainly concerned with fabrication of graphitized bulk microstructures in diamond using femtosecond and picosecond lasers and investigations of their properties, and these studies were oriented to applications in photonics [8–10, 12] and diamond gem marking [13, 14].

Recently, we reported two findings characteristic of the bulk microstructuring of single-crystal diamond with visible and UV picosecond pulses, namely, the crystallographic-plane dependent character of the structural modifications and appearance of the 3H luminescence in ps-laser-

irradiated diamond [15, 16]. The effect of crystallographic orientation is pronounced in that the ps-laser-induced phase transformations are initiated along {111} planes known as the planes of the lowest strength in diamond crystals [17]. Also such a behavior of laser-induced bulk modifications was suggested [15] to be alike for ultrashort pulses of different duration (in the range from 10 ps to 120 fs) that follows from a similar morphology of the bulk microstructures produced by femtosecond pulses [10, 11]. It is clear that the crystallographic-plane dependence of bulk modifications in single-crystal diamond is an important factor in microstructuring with ultrashort pulse lasers and its mechanism is based on the strength anisotropy of diamond, so further studies are needed for deeper understanding of the mechanism and gaining new knowledge of how to control the microstructuring along the {111} planes. It should be emphasized that herein we consider the laser-induced structural changes (graphitization, amorphization) which can occur in the bulk of diamond [18] and can lead to generation of high internal stresses, which however do not exceed the fracture strength of diamond and do not cause catastrophic mechanical damage [16] of diamond single crystals.

Another point of interest in the experiments on picosecond-laser interaction with type IIa single-crystal diamonds deals with generation of stimulated Raman scattering (SRS) and efficient conversion of the incident laser light to Stokes and anti-Stokes radiation [19–23]. The studies of the SRS in diamond have showed high potential of diamond single-crystals (produced by chemical vapor deposition (CVD) technology) for development of Raman laser devices; current achievements in the design and performance of CVD-diamond Raman lasers are summarized in a recent review paper by Mildren et al. [24].

The Raman scattering effects are the intrinsic properties of the material which are strongly pronounced during multipulse irradiation at increasing laser intensities prior to the laser-induced breakdown in the bulk of diamond, and therefore they can give valuable information on the pre-breakdown state of diamond under picosecond-laser irradiation. In the SRS process [25], the incident laser radiation is the energy source and due to nonlinear coupling effects its energy is transferred to the Raman radiation and the phonons, and also to higher order Stokes and anti-Stokes radiations. Therefore, the energy balance in the laser-diamond coupling is changing, that may affect the conditions of laser-induced breakdown and bulk microstructuring. Secondly, measurements of the SRS spectra during multipulse laser irradiation can be applied to determine a local temperature of diamond in the beam waist using the intensity ratio of the Stokes to anti-Stokes lines [26, 27]. To determine the temperature of a laser-irradiated microscopic region in the bulk of transparent materials is really a difficult task, so experimental data is lacking except for one recent paper in which an experimental approach is proposed for the temperature measurements in the femtosecond-laser-irradiated diamond using the pump-probe interferometric technique [28]. And finally, laser-induced bulk modifications can change the Raman scattering efficiency and the resulting spectra that were really observed in our previous experiments with UV ps-laser when the formation of a bulk microstructure in diamond resulted in dramatic changes in the SRS behavior [16]. Considering also the photoluminescence (PL) effects due to various defect centers in diamond (NV luminescence, 3H luminescence observed in the previous experiments [15, 16]), the idea was to install a spectrophotometer into the experimental setup and to monitor the ps-laser-induced PL spectra in the course of multipulse irradiation in the bulk of diamond.

In the paper we report on picosecond-laser bulk microstructuring and stimulated Raman scattering in CVD single-crystal diamond during multipulse irradiation at $\lambda = 532$ nm wavelength. In the studies we focus on the following interrelated tasks: (i) effect of the crystal orientation (relative to the direction of the incident laser beam) on the character of bulk modifications, laser-induced breakdown thresholds (thresholds of microstructure formation) and SRS lasing in diamond, (ii) effect of the pulse duration ($\tau_1 = 10$ ps and $\tau_2 = 44$ ps) on the laser-induced breakdown thresholds and generation of high-order Stokes and anti-Stokes radiations, (iii) estimation of the local temperature of ps-laser-irradiated regions in the bulk of diamond based on the Stokes to anti-Stokes intensity ratios in the spectra, and the efficiency of energy conversion of the incident laser light to the backscattered Raman radiation.

## 2 Experimental details

The bulk modification/microstructuring of diamond was carried out using a picosecond MOPA (master-oscillator power-amplifier) laser system—the DUETTO$^{TM}$ laser system [29], which has demonstrated excellent performance in microprocessing of metals and dielectric materials [30]. This picosecond-laser system generates pulses of 10 ps duration, the repetition rate can be varied between 50 kHz and 1 MHz, and the maximum average power is 10 W. The beam quality is $M^2 < 1.3$.

Type IIa CVD single-crystal diamond plates of 6.0 mm × 1.34 mm × 1.26 mm size (length × width × thickness), with mechanically polished {100} growth faces and {110} side faces, nitrogen content $[N] < 1$ ppm (from Element Six Ltd [31]), were used as the samples for ps-laser microstructuring. The CVD diamond single-crystals are characterized by high crystalline and optical quality, as reported elsewhere [32, 33].

The experimental setup for ps-laser bulk microstructuring and observation of stimulated Raman effects in diamond

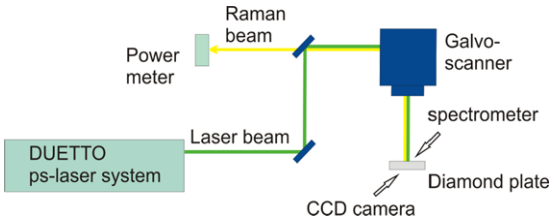


**Fig. 1** Experimental setup for ps-laser microstructuring of diamond crystals, equipped with a video imaging system and photoluminescence (PL) measuring setup

crystals is shown schematically in Fig. 1. As a laser source, we used the second laser harmonic of the DUETTO system which generates picosecond pulses at the wavelength $\lambda_0 = 532$ nm. In our studies of the ps-laser-induced SRS lasing two pulse durations ($\tau_1 = 10$ ps and $\tau_2 = 44$ ps) were used, both values being larger than the phonon lifetime ($\tau_R = 6.8$ ps [34]) in diamond. The longer pulse duration of 44 ps was realized by introducing an etalon into the seed laser of the DUETTO system. The laser pulse energy was in the range of $\varepsilon = 0.2$ μJ to $\varepsilon = 5$ μJ; the pulse repetition rate was $f = 50$ kHz (in some experiments it was varied from 50 to 300 kHz, and from 50 down to 5 kHz). A laser beam was focused using a galvo-scanner equipped with a 100-mm $f$–$\theta$ objective, the laser beam radius in the focal plane of the objective was $w_o = 7$ μm.

A video imaging system (model "Digital viewer GE-5") was applied for real-time observation of the appearance and growth of a laser-modified region in the bulk of diamond in the course of multipulse irradiation, as described and demonstrated elsewhere [15]. In the experiments, the laser beam was focused through a diamond plate either to the rear side of the plate or 0.5–0.8 mm beyond the crystal. Focusing the laser beam to the backside interface provides lower threshold values of the optical breakdown than that in the bulk of diamond due to interference of incident and reflected light waves at the back interface [1, 35]. Also this makes bulk microstructure formation and growth more reproducible and enables us to have access (from the back side of the diamond plate) to laser-modified diamond for structural investigations using Raman and PL spectroscopy techniques [15, 16]. The latter focusing conditions were aimed at increasing pulse energy and average power of the incident laser beam (avoiding the laser-induced breakdown at the backside surface) in the course of SRS measurements. The sample translation velocity (in the direction of a laser beam) was $V_z = 0$ in all tests, i.e. the focus position was fixed, so the growth of a bulk 'graphitized' microstructure from the rear side towards the laser beam was controlled by the laser intensity and the conditions of the ionization wave propagation in the bulk of diamond, as was discussed elsewhere [2].

In addition, a PL measurement setup has been installed into the experimental setup of bulk microstructuring in order to monitor the ps-laser-induced PL spectra in the course of multipulse irradiation and structure modification in the bulk of diamond. We call the measured spectra as PL spectra, implying that all ps-laser-induced processes of light emission and scattering in diamond (NV luminescence, Raman emission/scattering, and Rayleigh scattering) are registered. Emitted/scattered light is collected with a lens (normally to the laser beam) and is sent through a notch filter to a USB650 Red Tide Spectrometer to obtain a PL spectrum of a local volume in the bulk of the crystal. The Red Tide is a small-footprint lab spectrometer; it has a wavelength range of 350–1000 nm, and utilizes a detector with 650 active pixels (i.e. one data point per nanometer), and offers ~2.0 nm optical resolution [36].

## 3 Results and discussion

### 3.1 Picosecond-laser-induced breakdown in diamond during multipulse irradiation

In the experiments of ps-laser bulk microstructuring, irradiation conditions were defined by (i) focusing a laser beam through a diamond plate to the rear side of the plate, (ii) the pulse repetition rate of $f = 50$ kHz, and (iii) the sample translation velocity $V_z = 0$ in the direction of a laser beam (i.e. position of the focal plane was fixed at the backside of diamond plates). The value of the pulse energy (or incident laser fluence) corresponding to the microstructure formation at the back side of the sample was determined as a bulk microstructuring threshold ($\varepsilon_{th}$) which was dependent on other irradiation parameters, particularly, the pulse duration and crystal orientation (to be discussed below). As mentioned above, the true threshold values of laser fluence/intensity (or breakdown field strength) corresponding to initiation of the optical breakdown at the back side surface should be higher than the $\varepsilon_{th}$ values due to interference of incident and reflected light waves at the back interface [1, 35].

The growth of a bulk "graphitized" microstructure from the rear side towards the laser beam is controlled by the pulse energy, as was discussed in our previous papers on femtosecond laser microstructuring in the bulk of diamond [2, 10]. A similar dependence of the growth rates on the pulse energy was observed for bulk microstructuring with ps-laser [15]. Under the conditions of $\varepsilon \geq \varepsilon_{th}$ and $V_z = 0$, the microstructure grows from the backside surface ($z = 0$) to a certain distance $z = z^*(\varepsilon)$ in the bulk of the diamond crystal, the resulting length of the microstructure being dependent on the pulse energy. Figure 2 shows an optical microscopy image of bulk microstructures fabricated in a 1.34-mm-thick diamond plate by 10-ps pulses of different energies from $\varepsilon = 0.5$ μJ to $\varepsilon = 2.0$ μJ at $f = 50$ kHz, which evidences that the length increases with the pulse energy.

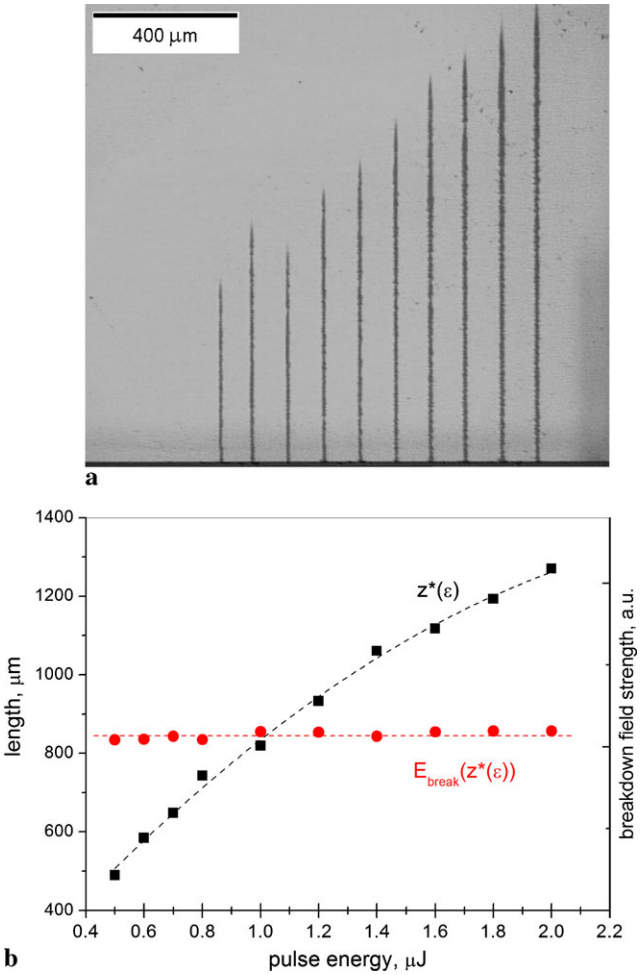


**Fig. 2** (**a**) Optical image of bulk microstructures fabricated in a 1.34-mm-thick diamond plate by ps-laser irradiation ($\lambda = 532$ nm, $\tau = 10$ ps) at different pulse energies of $\varepsilon = 0.5$, 0.7, 0.6, 0.8, 1.0, 1.2, 1.4, 1.6, 1.8 and 2.0 μJ (from *left* to *right*), $f = 50$ kHz, $V_z = 0$; the laser beam incidence along [110] direction. (**b**) Dependence of the length $z^*(\varepsilon)$ of bulk microstructures on the pulse energy (*squares*), and calculated breakdown field strength (*circles*) $E_{\text{break}} \propto [\varepsilon/(1 + (z^*/z_R)^2)]^{1/2}$ at the tip of each microstructure (see text for details)

For the data in Fig. 2, the laser beam incidence was along [110] direction, and the bulk microstructuring threshold was $\varepsilon_{\text{th}} = 0.5$ μJ.

The process of the laser-induced structure growth can be considered as a "self-supported" propagation of the ionization and structure transformation ("graphitization") waves into the bulk of diamond unless it stops at a distance $z = z^*(\varepsilon)$. The mechanism of such a propagating optical breakdown implies that multipulse irradiation of a local laser-damaged (graphitized) region leads to ionization of defect/impurity states and injection of the seed electrons into a neighboring undamaged region (e.g. via ballistic movement, hot electron diffusion [2]) for the avalanche ionization and structure transformation to occur. So the graphitized microstructure continues to grow into the bulk of diamond unless the local laser intensity at the front of the growing structure becomes less a certain threshold value required for optical breakdown. It is logical to expect that the threshold laser intensity (or breakdown field strength) should be the same at the tip (i.e. at $z = z^*(\varepsilon)$) of each microstructure produced at different pulse energies in the range from $\varepsilon = 0.5$ μJ to $\varepsilon = 2.0$ μJ.

In our estimation of the threshold laser intensity and breakdown field strength at $z = z^*(\varepsilon)$, we use standard expressions for the Gaussian beam intensity distribution and beam parameters (beam width, Rayleigh length), taking into account the beam quality of $M^2 < 1.3$.

The intensity distribution along the beam axis is given by the expression

$$I(z) = I_0\big[w_0/w(z)\big]^2, \tag{1}$$

where $I_0$ is the intensity at the center of the beam at its waist, $w_0$ is the focal spot radius, and $w(z)$ is the beam width as a function of the axial distance $z$.

The variation of the beam width $w(z)$ along the beam axis is given by

$$w(z) = w_0\big[1 + (z/z_R)^2\big]^{1/2}, \tag{2}$$

where $z_R$ is the Rayleigh length (for free space, $z_R = \pi w_0^2/\lambda$). In diamond, the depth of focus is increased by a factor of $n = 2.4$, so for the experimental conditions used during bulk microstructuring the Rayleigh length is

$$z_R = n\big(\pi w_0^2/M^2\lambda\big) \tag{3}$$

For $\lambda = 532$ nm and $w_0 = 7$ μm, the Rayleigh length is $z_R = 534$ μm.

Then, replacing $I_0$ in (1) by $I_0 \approx \varepsilon(1 - R)/\pi w_0^2\tau$ ($R = 0.17$, $R$ is the reflection from the front surface, $\tau = 10$ ps), we obtain the following expressions for estimation of the threshold laser intensity ($I_{\text{th}}$) and breakdown field strength ($E_{\text{break}}$) at the tip of each microstructure at $z = z^*(\varepsilon)$:

$$I_{\text{th}}\big(z^*(\varepsilon)\big) = A\varepsilon/\big[1 + \big(z^*/z_R\big)^2\big], \tag{4}$$

$$E_{\text{break}}(z^*(\varepsilon)) = (I_{\text{th}} Z_0/n)^{1/2}[1], \tag{5}$$

where $\varepsilon$ is taken in μJ (in the range from 0.5 to 2.0 μJ), $A = 5.65 \times 10^{10}$ W/cm$^2$, and $Z_0 = 377$ Ω is the free-space impedance.

Two dependences are plotted in Fig. 2b: (1) the dependence of the structure length ($z^*$) on the pulse energy (the length is determined from Fig. 2a), and (2) the dependence of the breakdown field strength on the pulse energy as $E_{\text{break}} \propto [\varepsilon/(1 + (z^*/z_R)^2)]^{1/2}$. It is seen that $E_{\text{break}} = const$ at the tip of each microstructure formed in the bulk of diamond. This important result underlines that the dielectric breakdown mechanism is the main mechanism governing the picosecond-laser-induced optical breakdown and bulk modifications of diamond during multipulse irradiation.

From (4) and (5), the estimation of the threshold laser intensity and breakdown field strength gives the values of $I_{th} = 17$ GW/cm$^2$ and $E_{break} = 1.6$ MV/cm, which are appreciably lower than the breakdown thresholds previously reported [1]. The fact of lowering of the optical breakdown thresholds ensues from the discussed-above mechanism of the "self-supported" structure growth towards the laser beam during multipulse irradiation. The presence of a local laser-modified region in the bulk promotes the generation and injection of the seed electrons into an undamaged region for the electron avalanche, which lowers the optical damage threshold compared to that of the original, defect-free diamond. That is, if a local defect region is intentionally formed in the bulk of diamond, it may serve as a starting point of a three-dimensional microstructuring of the diamond crystal at laser intensities which can be much lower than the intrinsic breakdown threshold of the material.

### 3.2 Effect of crystallographic orientation on the character of bulk modifications and ps-laser-induced Raman scattering

In all previous experiments on the bulk microstructuring of diamond crystals with visible and near-infrared ultra-short laser pulses [2, 10–12, 15] a laser beam was incident normally to the polished {100} top faces. Under the [100] beam incidence, laser-induced structural modifications in the bulk were shown to propagate preferably along {111} planes [15]. These bulk modifications were more distinctly pronounced during UV ps-laser microstructuring of diamond [16]. In addition, the experiments with UV ps-laser ($\lambda = 355$ nm) have demonstrated that the direction of the laser beam incidence relative to a given crystallographic direction (⟨100⟩ or ⟨110⟩) in the diamond plates influences the crystallographic-plane dependent character of bulk modifications [16].

In this paper we focus on the effects of the laser beam incidence (along [100] or [110] direction) on the formation and morphology of bulk microstructures and generation of stimulated Raman emission during multipulse irradiation with visible picosecond pulses. Figure 3 compares the morphology of two bulk microstructures produced at the same laser irradiation parameters (irradiation with 10-ps pulses of $\varepsilon = 1$ μJ, $f = 50$ kHz, $P = 50$ mW) and two different crystal directions, [100] and [110], of the laser beam incidence. A left image of each couple (a, b and c, d) in Fig. 3 is related to a local region in the bulk (at about several hundred microns from the backside surface) and a right image is that of the tip of the microstructure located at ~800 μm from the backside (as seen from Fig. 2). It is interesting to note that the crystallographic-plane dependent character of the bulk modifications is most clearly pronounced in the regions close to the tips of microstructures where the laser intensity and local temperature are the lowest ones and the

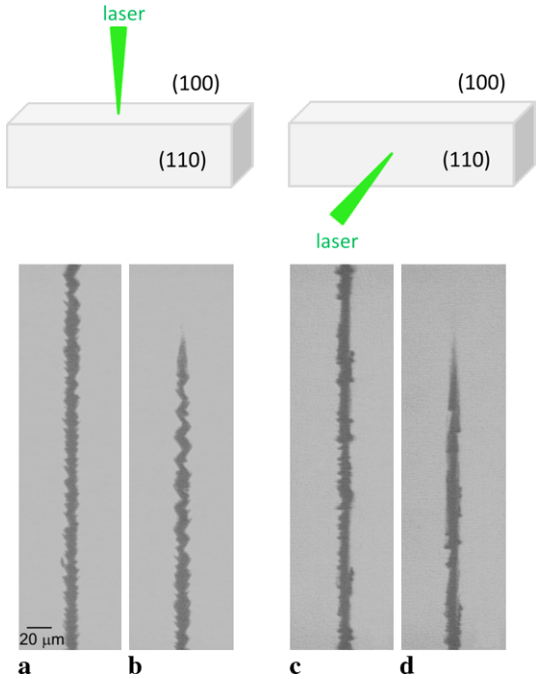


**Fig. 3** Schematic view of two irradiation regimes with the laser beam incidence along the [100] and [110] directions, and optical images of the bulk microstructures fabricated at $\varepsilon = 1$ μJ and $f = 50$ kHz; (**a**, **b**) Two regions of the microstructure produced at the [100] beam direction, and (**c**, **d**) two regions of the microstructure produced at the [110] beam direction

laser-induced optical breakdown is controlled by the electric field strength (shown in Fig. 2 and discussed above). As follows from Fig. 3, changing the direction of the laser beam incidence (from [100] to [110]) strongly influences the microstructure formation in the bulk of diamond. Assuming the structure transformation to start along the {111} planes [15], it is however difficult to answer which of the {111} planes are involved in constructing the optical images shown in Fig. 3. If, for instance, we consider an unpolarized laser beam incident onto the cube face (001), then the four {111} planes the beam irradiates are to be equivalent, but viewing the microstructure from the [110] direction makes "visible" only two of the {111} planes, i.e. (111) and $(\bar{1}\bar{1}1)$, and not observable two other planes $(1\bar{1}1)$ and $(\bar{1}11)$. The bulk microstructures produced along the [110] direction are viewed from the [001] direction, that makes the process and mechanism of bulk modifications less evident than that for the [001] beam incidence. So the data of viewing from other directions is needed to get a true 3D image of the produced microstructures and to determine contribution of the {111} planes to the optical contrast observed, and to clarify the effect of laser beam incidence on crystallographic-plane dependent bulk modifications in single-crystal diamond.

For both the [100] and [110] directions of the beam incidence, the threshold of the bulk microstructure formation at the backside surface was determined to be practically the

same and equal to $\varepsilon_{th} = 0.5$ μJ, which corresponds to irradiation with 10-ps pulses at $f = 50$ kHz and focusing the laser beam to the rear side of the sample. For Raman scattering measurements, the laser beam was focused 0.5–0.8 mm beyond the crystal, which enabled us to increase the laser beam size, the pulse energy and average power of the incident laser radiation, and therefore the scattering cross section and Raman signal intensity, with the laser intensities being lower the threshold of optical breakdown at the backside surface.

PL spectra measured during multipulse irradiation at the beam incidence along [100] direction and different laser powers from 50 to 750 mW are displayed in Fig. 4. All the spectra contain (i) a low-intensity peak of the scattered laser light at $\lambda_0 = 532$ nm (due to very low transmission of a notch filter at $\lambda_0 = 532$ nm), (ii) a broad band of the NV luminescence [37] in the spectral range 550–750 nm, and (iii) a Raman line (first Stokes line) at the wavelength $\lambda_{1S} = 572.6$ nm. The 1st Stokes line intensity increases linearly with the laser power (as well as other spectral lines), which is typical of the spontaneous Raman scattering in diamond [19].

It is known that the Raman scattering efficiency is dependent on crystal orientation, the analysis of its dependence on incident and Stokes beam polarizations for several beam directions in diamond single crystals is given in Ref. [33]. In our experiments with an unpolarized laser beam, the effect of crystal orientation on the Raman lasing behavior was also observed (and most strongly pronounced for longer ps pulses). Figure 5 shows a PL spectrum recorded during ps-laser irradiation at the [110] beam incidence and pulse energy of $\varepsilon = 3$ μJ ($f = 50$ kHz, $P = 150$ mW) before the microstructure formation at the back side of the sample. One can see from Fig. 5 that the 1st Stokes intensity exhibits a nonlinear increase with laser power at $P > 100$ mW (shown in the inset in Fig. 5) and that the 1st anti-Stokes and 2nd Stokes lines have appeared in the spectrum, which are indicative of generation of the SRS in the diamond crystal.

During ps-laser irradiation a local volume of ~200 μm size in the bulk was probed to get the resulting PL spectra (in the current experiments it was located around the laser beam at 0.4–0.5 mm from the back side of the sample). So using the PL setup integrated into the ps-laser system makes it possible to determine (estimate) the temperature of local laser-irradiated regions in the bulk of diamond, based on the intensity ratio of the 1st Stokes line to the 1st anti-Stokes line in the recorded spectrum. The application of Raman scattering spectroscopy for noncontact temperature measurements of diamond and other materials was reported elsewhere [26, 27, 38, 39], but the procedure was demonstrated for the samples uniformly heated to high temperatures rather than for local microscopic regions in the bulk of a transparent material.

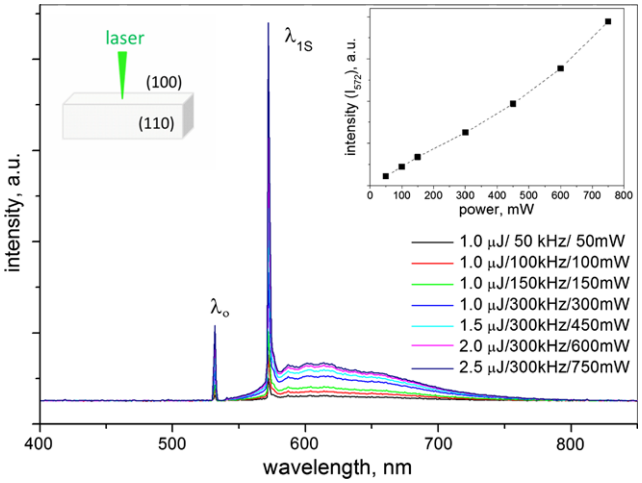


**Fig. 4** PL spectra measured during ps-laser multipulse irradiation at different laser powers ranged from 50 mW to 750 mW. Pulse duration is $\tau_1 = 10$ ps, laser beam incidence is along [100] direction, focus position is 0.8 mm beyond the diamond plate; $\lambda_0 = 532$ nm is the laser wavelength, $\lambda_{1S} = 572.6$ nm is the 1st Stokes wavelength. An *inset* shows the dependence of the intensity of the 1st Stokes line on the laser power

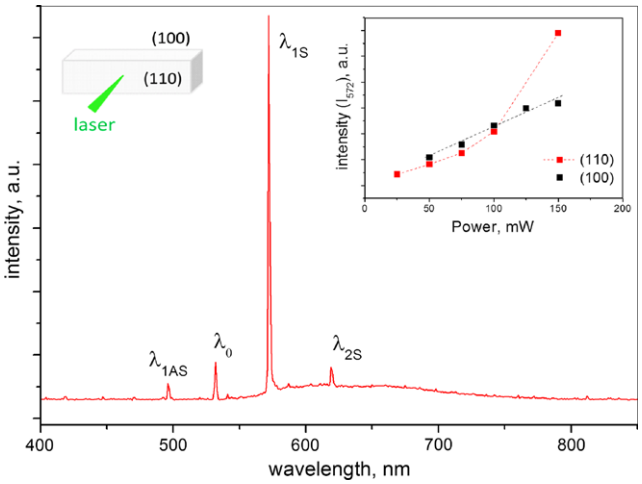


**Fig. 5** PL spectrum measured during ps-laser irradiation at $\varepsilon = 3$ μJ/$f = 50$ kHz/$P = 150$ mW before microstructure formation. Pulse duration is $\tau_1 = 10$ ps, laser beam incidence is along [110] direction, focus position is 0.5 mm beyond the diamond plate; $\lambda_{1S} = 572.6$ nm, $\lambda_{2S} = 620$ nm, and $\lambda_{1AS} = 496.8$ nm are the 1st Stokes, 2nd Stokes, and 1st anti-Stokes wavelengths. An inset shows the dependence of the intensity of the 1st Stokes line on laser power for [110] and [100] beam directions

The ratio of intensities of the 1st Stokes ($I_S$) and the 1st anti-Stokes ($I_{AS}$) lines is determined [26, 27] as

$$\frac{I_S}{I_{AS}} = \left(\frac{\nu_0 - \nu_p}{\nu_0 + \nu_p}\right)^4 e^{(h\nu_p/kT)} \tag{6}$$

where $\nu_0$ is the laser frequency, $\nu_p$ is the phonon frequency, $T$ is the temperature of a local laser-irradiated region in the bulk, and $h$ and $k$ are the Planck and Boltzmann constants.

For the laser wavelength $\lambda_0 = 532$ nm and laser frequency $\nu_0 = 18797$ cm$^{-1}$, phonon frequency $\nu_p = 1332$ cm$^{-1}$ and the ratio $I_S/I_{AS} = 24$ (from the PL spectrum in Fig. 5), we obtain $T = 511$ K. This estimated value is related to the bulk local temperature at about 0.4–0.5 mm away from the back side where the laser breakdown occurs during continuing irradiation with 10-ps pulses at $\varepsilon = 3$ μJ/$f = 50$ kHz/$P =$ 150 mW (i.e. conditions of measurements of the PL spectrum in Fig. 5). Further testing of the PL measurement procedure (e.g. to check if the PL spectra and intensity ratio $I_S/I_{AS}$ change along the beam axis) and modeling of bulk heating with high-repetition rate ps-lasers are needed to verify the applicability of the proposed technique for local temperature measurements, as compared with other methods reported for diamond and other transparent materials [28, 40, 41].

### 3.3 Effects of crystal orientation and pulse duration on the SRS lasing and ps-laser-induced breakdown in diamond

In this section we report on using longer picosecond pulses, of 44 ps duration, to study the effects of crystal orientation on the bulk microstructuring and stimulated Raman scattering in diamond. Figure 6 and Table 1 present comparative data of the thresholds of bulk microstructure formation for the [100] and [110] beam directions. Three important results follows from the presented data.

First, the threshold values of the laser-induced breakdown and microstructure formation (at the back interface) for the [100] beam direction agree with the scaling law of the fluence breakdown threshold $\varepsilon_{th} \propto (\tau)^{1/2}$ valid for the pulse durations $\tau \geq 10$ ps [3]. Second, the breakdown thresholds for the [110] beam direction are considerably larger (on average, by a factor of 3) than those for the [100] beam incidence. These threshold values do not follow the scaling law $\varepsilon_{th} \propto (\tau)^{1/2}$, though the breakdown thresholds during multipulse irradiation with 10-ps pulses were practically the same for both the [100] and [110] beam directions, i.e. $\varepsilon_{th} \approx 0.5$ μJ (for $\tau_1 = 10$ ps and $w_o = 7$ μm). And third, a large scatter in the threshold values was observed.

The observed difference in the breakdown thresholds for two crystal orientations correlates with a very different behavior of the SRS generation and will be discussed below. The large scatter in the threshold data can be attributed to dependence of the breakdown threshold on the presence of seed electrons for the avalanche process [4]. For high-quality CVD diamond crystals with very low concentration of impurities it makes very probable that small changes in the number of seed electrons in the focal volume can strongly influence the process of avalanche ionization and therefore lead to a large scatter in the breakdown thresholds at different bulk regions in the crystal.

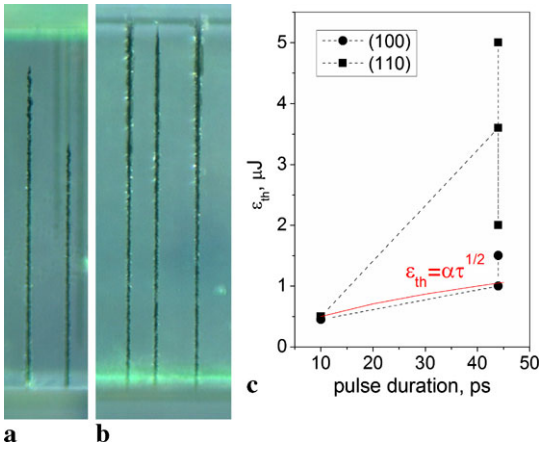


**Fig. 6** Bulk microstructures produced with 44-ps pulses at the [100] beam direction (structures 1 and 2 from *left* to *right*) (**a**) and at [110] beam direction (structures 1, 2, and 3 from *left* to *right*) (**b**); thresholds of bulk microstructure formation for two pulse durations $\tau_1 = 10$ ps and $\tau_2 = 44$ ps and two beam directions (**c**)

**Table 1** Data of the thresholds of bulk microstructure formation during multipulse irradiation with 44-ps pulses at the [100] and [110] beam directions and $f = 50$ kHz. The microstructures are shown in Fig. 6(a, b). The plate thickness for the [100] direction is 1.26 mm and for the [110] direction is 1.34 mm

| Structure No. | Beam direction | $\varepsilon_{th}$, μJ | Structure length, mm |
|---|---|---|---|
| Structure 1 | [100] | 1.5 | 1.14 |
| Structure 2 | [100] | 1.0 | 0.86 |
| Structure 1 | [110] | 3.6 | 1.34 |
| Structure 2 | [110] | 2.0 | 1.3 |
| Structure 3 | [110] | 5.0 | 1.34 |

PL spectra measured during 44-ps-laser irradiation of the diamond (100) and (110) faces are shown in Figs. 7 and 8. For the [100] beam direction (Fig. 7), an intense 1st Stokes line at $\lambda_{1S} = 572.6$ nm and very weak signals of the 1st anti-Stokes and 2nd Stokes components are generated at the incident laser intensities close (but lower) to the breakdown threshold and microstructure formation at the back side of the plate.

For the [110] beam direction (Fig. 8), the SRS lasing is much more efficient which is pronounced in generation of high-order Stokes and anti-Stokes radiation of high intensity. Particularly, the 1st, 2nd and 3rd Stokes, the 1st and 2nd anti-Stokes lines are generated at the wavelengths $\lambda_{1S} = 572.6$ nm, $\lambda_{2S} = 620$ nm, $\lambda_{3S} = 675.6$ nm, $\lambda_{1AS} =$ 496.8 nm and $\lambda_{2AS} = 466$ nm, respectively. It should be noted that the Red Tide Spectrometer is characterized by saturation at about 4000 a.u., so the PL spectra (in Fig. 8) are presented, first of all, to show considerably increased intensities of the Stokes and anti-Stokes lines rather than most intense 1st Stoke radiation. Figure 8b summarizes the data

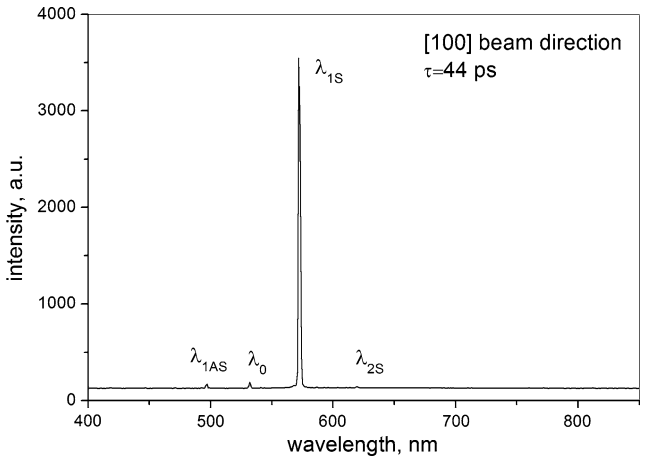


**Fig. 7** PL spectrum measured during 44-ps-laser irradiation of diamond at the [100] beam direction and $\varepsilon = 2.6$ μJ/$f = 50$ kHz/$P = 130$ mW (before bulk damage at $\varepsilon_{th} = 2.8$ μJ); focus position is 0.5 mm beyond the sample

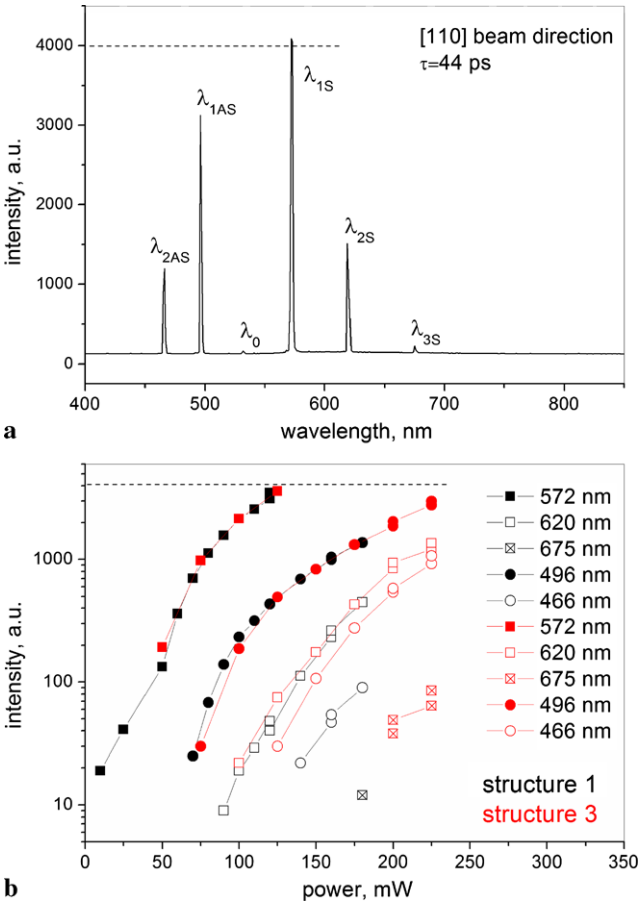


**Fig. 8** (**a**) PL spectrum measured during 44-ps-laser irradiation of diamond at the [110] beam direction and $\varepsilon = 4.5$ μJ/$f = 50$ kHz/$P = 225$ mW (structure 3, before bulk damage at $\varepsilon_{th} = 5$ μJ); $\lambda_0 = 532$ nm is the laser wavelength, $\lambda_{1S} = 572.6$ nm, $\lambda_{2S} = 620$ nm, $\lambda_{3S} = 675.6$ nm, $\lambda_{1AS} = 496.8$ nm, $\lambda_{2AS} = 466$ nm are the generated high-order Stokes and anti-Stokes wavelengths. (**b**) Intensities of the Stokes and anti-Stokes lines in the PL spectra measured before bulk damage at $\varepsilon_{th} = 3.6$ μJ (structure 1) and $\varepsilon_{th} = 5$ μJ (structure 3). *Dashed lines* show the saturation value of the spectrometer

of the PL spectra recorded for the structures 1 and 3 (i.e. before the structure formation, see Fig. 6b and Table 1) during irradiation at [110] beam direction and demonstrates the SRS lasing behavior with increasing laser power.

The observed difference in the SRS lasing during ps-laser irradiation at the [110] beam direction and two pulse durations $\tau_1 = 10$ ps and $\tau_2 = 44$ ps (compare SRS spectra in Fig. 5 and Fig. 8) is supposed to be caused by the transient behavior of the SRS for $\tau_1 = 10$ ps which results in an increase of the SRS threshold [42].

As soon as the laser breakdown occurs and graphitized structure is formed in the bulk or through the diamond plate (see Fig. 6, a and b), PL spectra are strongly changed as compared to those measured prior to the laser damage and structure formation. Such changes in the PL spectra were observed in the course of irradiation with 44-ps pulses at $\varepsilon = 3.6$ μJ/$f = 50$ kHz/$P = 180$ mW (structure 1 formed along the [110] direction); the PL spectra obtained before and after the microstructure formation are shown in Fig. 9a. After the structure formation there is no more high-order Stokes and anti-Stokes lines present in the PL spectrum. Only a very weak signal of the first-order Raman line is observed due to the Raman scattering in the regions surrounding the bulk microstructure formed (excited by low-intensity edges of the incident Gaussian beam). At the same time, the integral intensity of the NV luminescence is greatly enhanced (especially, if we take into account that the intensity of the exciting laser beam is strongly decreased) and the appearance of the $[N–V]^-$ peak at $\lambda = 637$ nm is clearly observed. The latter fact indicates that the NV defects are charged presumably as a result of diffusion of free electrons generated in the avalanche ionization process.

The data of Fig. 8b were used to estimate the local temperature in the bulk (in a 200-μm-size region on the beam axis at about 0.5 mm from the back side) and its changes with increasing laser power, based on the calculation of the intensity ratio $I_S/I_{AS}$ (6) of the 1st Stokes and 1st anti-Stokes lines in the PL spectra. The temperature vs. laser power dependence is presented in Fig. 9b, it is related to 44-ps-laser irradiation at the [110] direction and laser powers $P \leq 120$ mW lower than the breakdown threshold $\varepsilon_{th} = 3.6$ μJ/$f = 50$ kHz/$P_{th} = 180$ mW (structure 1). Acquisition of the temperature data from the $I_S/I_{AS}$ ratio is limited to the power range of $P \leq 120$ mW because at $P > 120$ mW the 1st Stokes intensities are very high, reaching the spectrometer saturation and so making the determined $I_S/I_{AS}$ values incorrect.

It seen from Fig. 9b that the temperature rises with incident laser power to the value of $T = 750$ K (at $P = 120$ mW). With regard to the breakdown temperature, i.e. the temperature determined at $P_{th} = 180$ mW from a PL spectrum of

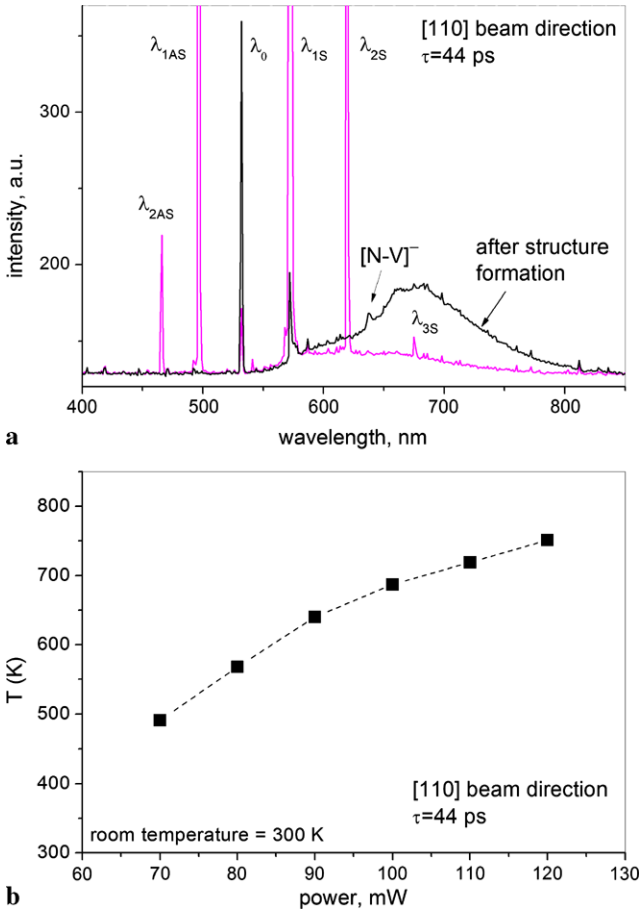


**Fig. 9** (**a**) PL spectra measured during 44-ps-laser irradiation of diamond at the [110] beam direction and $\varepsilon = 3.6$ μJ/$f = 50$ kHz/$P = 180$ mW before and after the bulk microstructure formation (structure 1); $\lambda_0 = 532$ nm is the laser wavelength, $\lambda_{1S} = 572.6$ nm, $\lambda_{2S} = 620$ nm, $\lambda_{3S} = 675.6$ nm, $\lambda_{1AS} = 496.8$ nm, $\lambda_{2AS} = 466$ nm are the generated Stokes and anti-Stokes wavelengths. (**b**) Temperature of a local laser-irradiated region in the bulk determined from the Stokes–to-anti-Stokes intensity ratio $I_{1S}/I_{1AS}$ (from the data of Fig. 8b)

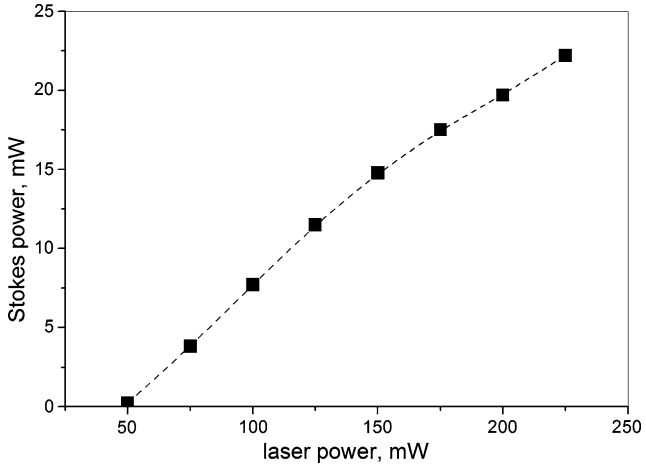


**Fig. 10** Dependence of the Stokes power on the laser power; power measurements were done during 44-ps-laser irradiation of diamond at the [110] beam direction simultaneously with the PL spectra measurements (data of the structure 3 in Fig. 8)

a bulk region close to the back interface, the value of $T = 750$ K seems to be appreciably underestimated. So the issues of accuracy and validity of temperature measurements using the proposed PL/Raman technique are important and require further investigations. The Raman spectroscopy technique enables a "self-calibration" of the temperature to be made by measuring the temperature-dependent shift of the first-order Raman line (the frequency decreases from 1332 $cm^{-1}$ at room temperature to 1318 $cm^{-1}$ at $T = 1000$ K [27]), but the spectral resolution of the Red Tide spectrometer used is not sufficient for this purpose. Nevertheless, the data of Fig. 9b are very important as they determine the lower limit of temperature in the focal volume ($T > 750$ K) and evidence the significant role of thermal effects in SRS processes induced by multipulse ps-laser irradiation.

The SRS data in Fig. 8 show that the generated 1st Stokes radiation at $\lambda_{1S} = 572.6$ nm is the most intense one in the PL spectra measured. This "yellow" Raman beam was found to be readily observed in the backward direction and the power of the backscattered Raman radiation was measured using a power meter placed behind a deflecting mirror as shown schematically in Fig. 1. The measurements were carried out during 44-ps-laser irradiation at the [110] direction simultaneously with the PL spectra measurements (see SRS data for structure 3 in Fig. 8). The dependence of the Stokes power on the laser power is shown in Fig. 10. The optical losses for the backscattered Raman beam (passing through Galvo scanner and deflecting mirror) are not known in the particular experimental scheme, so the obtained value of 10 % is considered as the lower limit of the conversion efficiency from the incident laser light to the backscattered Stokes radiation.

Taking into account the forward-backward asymmetry in the Stokes generation (i.e. forward-backward intensity ratio $>1$) [25] and also the energy transfer to higher order Stokes and anti-Stokes radiation, it can be concluded that the incident laser power is strongly depleted during the SRS lasing induced by 44-ps-laser irradiation at the [110] direction (shown in Figs. 8–9). The laser power depletion is thought to be a main reason of the significantly higher breakdown thresholds observed for the [110] direction as compared to the [100] direction.

## 4 Conclusions

Among the observed effects of the crystal orientation (the beam direction) and pulse duration on the bulk microstructuring and SRS lasing in single-crystal diamond, the following results are of interest and importance.

The analysis of the "length-on-pulse energy" dependence for bulk microstructures has surprisingly confirmed the fact of the constant breakdown field strength ($E_{\mathrm{break}} = const$) at the tips of the microstructures and evidenced the dominant mechanism in the processes of optical breakdown and bulk microstructuring of diamond during multipulse ps-laser irradiation.

It is found that the breakdown thresholds follow the known scaling law of ps-laser-induced damage in optical materials (i.e. threshold fluence scales as $\sim(\tau)^{1/2}$ for the pulse durations $\tau \geq 10$ ps), unless efficient high-order Stokes and anti-Stokes Raman lasing occurs in the crystal. This situation was found to take place for longer pulses ($\tau_2 = 44$ ps) and the beam direction [110], when the breakdown thresholds for the [110] beam direction proved to be $\sim$3 times the thresholds for the [100] direction. It is somewhat paradoxical that the higher is the efficiency of SRS lasing in diamond, the larger is the threshold of laser-damage in the bulk of diamond. This fact is a result of nonlinear coupling effects leading to laser power depletion, and it seems to be advantageous for diamond Raman laser applications.

Changing the direction of the laser beam incidence (from [100] to [110]) strongly influences the formation and morphology of bulk microstructures. Assuming the structure transformation to start along the {111} planes [15], it is however problematic to determine (based on the microscopy images obtained) contribution of each of {111} planes to the optical contrast observed, and to clarify the effect of the beam direction on crystallographic-plane-dependent bulk modifications in single-crystal diamond.

A method of local temperature measurements in the bulk of diamond based on the Stokes to anti-Stokes intensity ratio in the recorded SRS spectra is proposed. Preliminary data obtained with this method have showed the lower limit of temperature in the focal volume ($T > 750$ K) and evidenced the significant role of thermal effects in the SRS processes induced by multipulse ps-laser irradiation. Further investigations are needed to verify the applicability of the proposed PL/Raman technique for local temperature measurements in the bulk of diamond during multipulse irradiation.

The proposed experimental technique of combining an advance ps-laser system with a PL measuring setup has proved to be a very useful one for comprehensive study of ps-laser-induced processes in the bulk of diamond single crystals, including stimulated Raman scattering effects occurring at the "pre-breakdown" intensities and its interrelation with laser-induced bulk modifications occurring at and upon the breakdown.

**Acknowledgements** The authors are thankful to S.V. Garnov and I.I. Vlasov for helpful discussions of the SRS effects in diamond. The work was supported by the SNSF project IZ73Z0-128088/1.

## References

1. C.A. Klein, R. DeSalvo, Appl. Phys. Lett. **63**, 1895 (1993)
2. T.V. Kononenko, M. Meier, M.S. Komlenok, S.M. Pimenov, V. Romano, V.P. Pashinin, V.I. Konov, Appl. Phys. A **90**, 645–651 (2008)
3. D. Du, X. Liu, G. Korn, J. Squier, G. Mourou, Appl. Phys. Lett. **64**, 3071 (1994)
4. C.B. Schaffer, A. Brodeur, E. Mazur, Meas. Sci. Technol. **12**, 1784 (2001)
5. S. Preuss, M. Stuke, Appl. Phys. Lett. **67**, 338 (1995)
6. H.O. Jeschke, M.E. Garcia, K.H. Bennemann, Phys. Rev. B **60**, R3701 (1999)
7. A.A. Malyutin, S.V. Garnov, S.M. Pimenov, O.G. Tsarkova, V.I. Konov, in *ALT'02 International Conference on Advanced Laser Technologies*. SPIE, vol. 5147 (SPIE, New York, 2003), p. 33
8. Y. Shimotsuma, M. Sakakura, S. Kanehira, J. Qiu, P.G. Kazansky, K. Miura, K. Fujita, K. Hirao, J. Laser Micro Nanoeng. **1**, 181 (2006)
9. M. Shimizu, Y. Shimotsuma, M. Sakakura, T. Yuasa, H. Homma, Y. Minowa, K. Tanaka, K. Miura, K. Hirao, Opt. Express **17**, 46 (2009)
10. T.V. Kononenko, M.S. Komlenok, V.P. Pashinin, S.M. Pimenov, V.I. Konov, M. Neff, V. Romano, W. Lüthy, Diam. Relat. Mater. **18**, 196 (2009)
11. M. Neff, T.V. Kononenko, S.M. Pimenov, V. Romano, W. Lüthy, V.I. Konov, Appl. Phys. A **97**, 543 (2009)
12. T.V. Kononenko, V.I. Konov, S.M. Pimenov, N.M. Rossukanyi, A.I. Rukovishnikov, V. Romano, Diam. Relat. Mater. **20**, 264 (2011)
13. J.B. Ashcom Ph.D. thesis, Harvard University (2003). http://mazur-www.harvard.edu/sentFiles/Mazurpubs_309.pdf
14. A.A. Ionin, S.I. Kudryashov, K.E. Mikhin, L.V. Seleznev, D.V. Sinitsyn, Laser Phys. **20**, 1778 (2010)
15. S.M. Pimenov, I.I. Vlasov, A.A. Khomich, B. Neuenschwander, M. Muralt, V. Romano, Appl. Phys. A **105**, 673 (2011)
16. S.M. Pimenov, A.A. Khomich, I.I. Vlasov, E.V. Zavedeev, B. Neuenschwander, B. Jäggi, V. Romano, ALT Proc. **1** (2012). doi: 10.12684/alt.1.50
17. R.H. Telling, C.J. Pickard, M.C. Payne, J.E. Field, Phys. Rev. Lett. **84**, 5160 (2000)
18. V.N. Strekalov, V.I. Konov, V.V. Kononenko, S.M. Pimenov, Appl. Phys. A **76**, 603 (2003)
19. A.K. McQuillan, W.R.L. Clements, B.P. Stoicheff, Phys. Rev. A **1**, 628 (1970)
20. A.A. Kaminskii, R.J. Hemley, J. Lai, C.S. Yan, H.K. Mao, V.G. Ralchenko, H.J. Eichler, H. Rhee, Laser Phys. Lett. **4**, 350 (2007)
21. R.P. Mildren, J.E. Butler, J.R. Rabeau, Opt. Express **16**, 18950 (2008)
22. R.P. Mildren, A. Sabella, Opt. Lett. **34**, 2811 (2009)
23. D.J. Spence, E. Granados, R.P. Mildren, Opt. Lett. **35**, 556 (2010)
24. R.P. Mildren, A. Sabella, O. Kitzler, D.J. Spence, A.M. McKay, in *Optical Engineering of Diamond*, ed. by R.P. Mildren, J.R. Rabeau (Wiley-VCH, Weinheim, 2013), p. 239
25. Y.R. Shen, N. Bloembergen, Phys. Rev. **137**, A1787 (1965)
26. H. Herchen, M.A. Cappelli, Phys. Rev. B **43**, 11740 (1991)
27. J.B. Cui, K. Amtmann, J. Ristein, L. Ley, J. Appl. Phys. **83**, 7929 (1998)
28. V.V. Kononenko, E.V. Zavedeev, M.I. Latushko, V.I. Konov, Laser Phys. Lett. **10**, 036003 (2013)
29. K. Weingarten, Laser Tech. J. **6**(3), 51 (2009)
30. B. Neuenschwander, G.F. Bucher, C. Nussbaum, B. Joss, M. Muralt, U.W. Hunziker, P. Schuetz, Proc. SPIE **7584**, 75840R (2010)
31. www.e6cvd.com
32. I. Friel, S.I. Clewes, H.K. Dhillon, N. Perkins, D.J. Twitchen, G.A. Scarsbrook, Diam. Relat. Mater. **18**, 808 (2009)

33. R.P. Mildren, in *Optical Engineering of Diamond*, ed. by R.P. Mildren, J.R. Rabeau (Wiley-VCH, Weinheim, 2013), p. 1
34. F.C. Waldermann, B.J. Sussman, J. Nunn, V.O. Lorenz, K.C. Lee, K. Surmacz, K.H. Lee, D. Jaksch, I.A. Walmsley, Phys. Rev. B **78**, 155201 (2008)
35. M.D. Crisp, N.L. Boling, G. Dubé, Appl. Phys. Lett. **21**, 364 (1972)
36. www.oceanoptic.com
37. A. Wotherspoon, J.W. Steeds, P. Coleman, D. Wolverson, J. Davies, S. Lawson, J. Butler, Diam. Relat. Mater. **11**, 692 (2002)
38. R.J. Nemanich, D.K. Biegelsen, R.A. Street, L.E. Fennell, Phys. Rev. B **29**, 6005 (1984)
39. J. Niu, J. Sha, D. Yang, Scr. Mater. **55**, 183 (2006)
40. C.B. Schaffer, J.F. García, E. Mazur, Appl. Phys. A **76**, 351 (2003)
41. I. Miyamoto, K. Cvecek, M. Schmidt, Opt. Express **19**, 10714 (2011)
42. T.T. Basiev, A.A. Sobol, P.G. Zverev, V.V. Osiko, R.C. Powell, Appl. Opt. **38**, 594 (1999)